Computer Simulation of Dipolar-Depletion Colloids

by

© **Cassandra Clowe-Coish**

A thesis submitted in partial fulfillment of the requirements for the degree of Bachelor of Science.

Department of Physics & Physical Oceanography

Memorial University

April 2022

St. John's, Newfoundland and Labrador, Canada

Abstract

An experimental colloid-polymer mixture with an applied external electric field is subject to an induced dipole interaction and an effective attraction due to depletion of polymer in between close-approaching colloidal spheres. The electric field strength and polymer concentration affect the strength of these interactions and thus lead to distinct phase transitions and, more generally, a variation in local order with these parameters. A computational system replicating the experiment is developed to examine the static properties of the colloid, with greater spatial resolution in the direction of polarisation and increased control of parameters compared to experiment. Such an approach is adopted to attempt to resolve the question of decreased local order at high-polymer, high-field state points past a certain threshold, before which local order was observed to increase.

Acknowledgements

I would firstly like to thank my supervisor, Dr. Ivan Saika-Voivod, with whom I completed a summer internship in 2021 prior to beginning work on this thesis, giving me great insight into the fields of molecular dynamics simulation and of fluid thermodynamics. He provided much vital guidance and revision, and direction to resources. I would also like to acknowledge Shivani Semwal and Dr. Anand Yethiraj for providing key background information about the experiment, and for their assessment of simulation results. I also thank honours coordinator Dr. Mykhaylo Evstigneev for his guidance in the writing and presentation of this thesis.

I would also like to acknowledge Fred Perry, who set me up with a desktop computer and provided technical support.

Table of contents

List of figures

Chapter 1

Introduction

1.1   Overview of Computer Simulation of Molecular Systems

For physical systems involving many bodies, of great interest is the question of their behaviour at equilibrium subject to external constraints. The equilibrium properties of thermodynamic systems reveal not only qualities of materials, but also of the physics which govern their evolution. Much effort has gone into developing theoretical tools for probing the equilibrium state of such systems. Computer simulation is one such tool, favourable due to the high degree of control over system parameters. One approach to the simulation of many-body molecular systems is known as *molecular dynamics*. It is a method which evolves particles forward in time subject to a potential function, according to Newton's laws of motion. By examining the kinetic and potential energies, one can calculate characteristic thermodynamic properties, as well as produce static configurations of a system.

The field of molecular dynamics was pioneered by physicists Berni Alder and Tom Wainwright, along with programmer Mary Ann Mansigh Karlsen, as a deterministic alternative to Monte Carlo simulation of many-body systems[1]. Alder in particular was interested in the macroscopic behaviour of fluids generated by statistical means. In 1957, Alder and Wainwright simultaneously showed the efficacy of their new method and determined the existence of a first-order phase transition from fluid to crystal in a system of hard spheres, subject to the hard sphere interaction. The fluid phase was shown to become unstable at a high enough density threshold, at which point the crystal phase becomes favourable. Alder and Wainwright continued to study equilibrium properties of many-body systems, with Mansigh refining and optimising the code, and they later showed that the statistical behaviour of such systems is auto-correlated within short time intervals, i.e. the velocity of a particle at the current time is largely dependent on its velocity a short time ago, which is captured by deterministic simulation. This bolstered the validity of a molecular dynamics approach over stochastic simulation.[2]

As more powerful machines became readily available, the benefits of computer simulation as a tool of statistical mechanics became acutely apparent. Specifically, they are a way of obtaining a numerical solution to a theoretical problem with no closed-form analytical solution. In the modern era, they provide an algorithmic companion, or even alternative, to direct experiment. Physical theories can be tested in isolation within a program without having to account for undesired or uncontrolled empirical effects. The scale of the simulation is limited only by computing power, allowing for simulations of vast numbers of particles. In addition, one can simulate the bulk properties of a system by using periodic boundary conditions. Computer simulation can also sidestep the precision constraints of experimental apparatus, since the absolute time and length of the simulated system are limited only by machine

precision. Thus, computer simulation is apt for the study of the phase of materials comprised of microparticles, such as colloidal suspensions. In the experimental analog to the simulations detailed herein, for example, the configurations obtained from imaging phosphorescent polymer colloids lack resolution in the direction parallel with the applied electric field, which can be avoided altogether in computer simulation, since the three-dimensional position of all particles is always tracked.

1.2   Overview of Experiment

The experimental system being simulated is a suspension comprised of fluorescently labelled polymethyl methacrylate colloids 1.3 microns in diameter, dispersed in a solvent mixture of cyclohexyl bromide and cis-trans decalin of a density that closely matches that of the colloids. Non-adsorbing polystyrene is used to produce the depletion interaction, and a salt is added to screen the Coulomb interaction. The suspension is placed in a cell with electrodes at either end, whence the electric field is supplied. Three archetypal equilibrium configurations observed in experiment are of primary interest. Firstly, there is the fluid phase, which is exemplifies the natural behaviour of the system at weak field strength and low polymer concentration. Then, there is the highly ordered crystal phase, observed with strong electric field and intermediate polymer concentrations. Lastly, there is the disordered crystal or cluster phase, observed at high field values and high polymer concentration. It is observed that beyond a particular concentration threshold, at high field, the system no longer exhibits increasing order with increasing polymer concentration, but rather decreasing order [3]. The precise chemical setup need not be described in detail, since the interest lies primarily in the static equilibrium properties of the colloid subject to the characteristic

interactions, and not necessarily in precise measurements or predictions of thermodynamic properties. To determine the origin of the observed experimental results, it was essential to model the depletion interaction and the induced dipole-dipole interaction.

1.2.1 Hard Sphere Colloids and The Depletion Interaction

The depletion interaction is an effective attraction produced by an unbalanced osmotic pressure when two large colloidal particles approach each other closely enough that the interstitial space becomes depleted of the smaller, non-adsorbing polymer. It is preferable not to model the polymer explicitly, as this greatly increases computational complexity. Accounting for the effect of the polymers on the colloids through the depletion interaction allows one to explicitly simulate the colloidal particles alone. The depletion interaction is visualised in Figure 1.1. Further reading on the depletion interaction can be obtained in Asakura and Oosawa [4].

In general, a potential constructed to model the interactions between colloids starts with an approximation to hard-sphere repulsion: a steeply rising potential energy at a colloidal separation near σ, the colloid diameter. To model depletion interaction, there must additionally be a narrow potential well of width typically less than 10% of the diameter and of depth $\tilde{\epsilon}$. The dimensionless ratio $\epsilon = \tilde{\epsilon}/k_{\mathrm{B}}T$ governs whether colloids bond to each other and the longevity of those bonds. In simulations it is convenient to work with reduced units. For simplicity, $k_{\mathrm{B}}T$ is set to 1 in the computer simulation code. If $\tilde{T}$ is the physical temperature, the reported reduced temperature is $T = k_{\mathrm{B}}\tilde{T}/\tilde{\epsilon}$.

The potential chosen to model this colloidal system is a particular instance of a
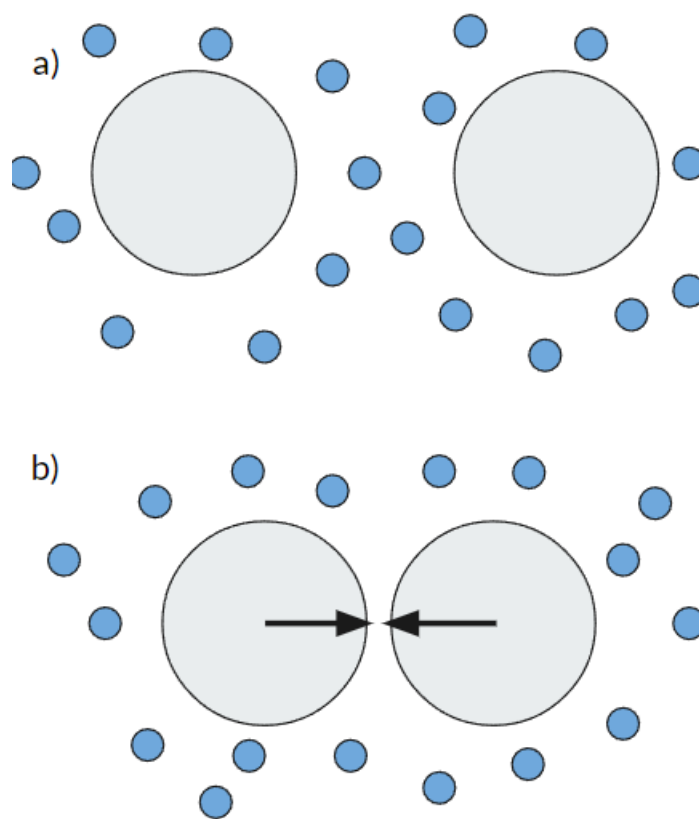
Figure 1.1: A visual representation of the depletion interaction. The grey circles represent the large colloidal particles, and the blue circles represent the small polymer spheres. In a), the two colloids are not experiencing much effective attraction, due to their relatively large separation. In b), however, the interstitial space between the colloids is depleted of polymer, and the result is an increased effective attraction due to the unbalanced fluid pressure on the colloids.

general short-range potential presented by Wang et al.[5],

$$U_c = \alpha\tilde{\epsilon} \left(\left[\frac{\sigma}{r}\right]^2 - 1 \right) \left(\left[\frac{r_c}{r}\right]^2 - 1 \right)^2 \tag{1.1}$$

$$F_c = \frac{2\alpha\tilde{\epsilon}}{r^3} \left[\sigma^2 \left(\left[\frac{r_c}{r}\right]^2 - 1 \right)^2 + 2r_c^2 \left(\left[\frac{\sigma}{r}\right]^2 - 1 \right) \left(\left[\frac{r_c}{r}\right]^2 - 1 \right) \right], \tag{1.2}$$

where r_c is the cutoff of the potential, and α is a normalisation parameter,

$$\alpha(r_c) = 2 \left(\frac{r_c}{\sigma}\right)^2 \left(\frac{3}{2\left(\left(\frac{r_c}{\sigma}\right)^2 - 1\right)} \right)^3 . \tag{1.3}$$

U_c is the potential energy of two particles separated by a distance r, and F_c determines the magnitude of the radial force between particles. F_c is positive for a repulsive force, and negative for attractive force.

The parameter r_c is, at the suggestion of the authors, set to 1.2σ to produce a narrow potential well, suitable for simulating the attraction between colloids due to polymer depletion. This potential is advantageous compared with the Lennard-Jones potential because it was constructed to be used in its standard form, as opposed to the Lennard-Jones potential, which has a broader well and is often cut and shifted to produce a potential of finite range, depending on the use case[5].

The location of the minimum of the potential, typically referred to as the "bond length," for this system is

$$r_{min} = r_c \left(\frac{3}{1 + 2\left(\frac{r_c}{\sigma}\right)^2} \right) . \tag{1.4}$$

Thus, for a colloidal system with $r_c = 1.2\sigma$, r_{min} is approximately equal to 1.055σ.

In these simulations, to model only the special case of zero polymer and zero field,
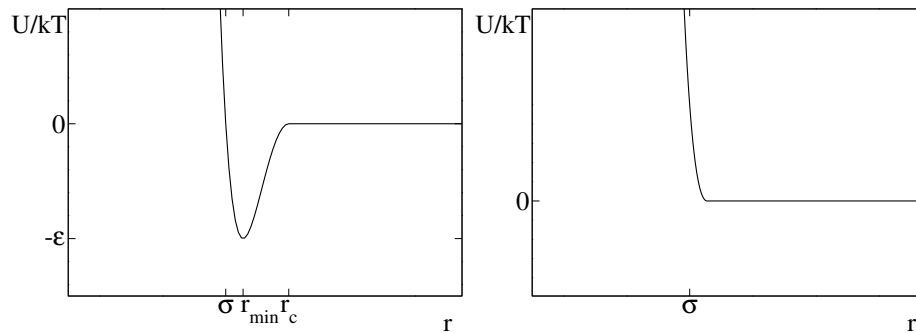
Figure 1.2: Graphs of the regular "colloid" potential (left), and the cut and shifted potential (right) used for modelling hard spheres. Note the narrow, finite attractive well in the normal case, and the steeply rising curve in the cut and shifted case. The right figure was generated by cutting the potential on the left at r_{min} and shifting it up to zero.

the colloid potential with $\epsilon = 1$ was cut at r_{min} and shifted up to zero, to maintain hard-sphere repulsion at this state point.

Graphs of the colloid potential in the normal case, and the hard-sphere case, are shown in Figure 1.2

This potential model was chosen since it is similar in structure to the Lennard-Jones potential, but its attractive well can be made narrower by adjusting the parameter r_c. The gradient within this well can therefore be made larger than that of the Lennard-Jones potential in order to simulate the effective attraction of the depletion interaction without needing to model polymer spheres explicitly. Furthermore, it allows for the adjustment of this parameter around the suggested value in future experiments, if necessary.

1.2.2 The Dipole Interaction

The second interaction to which the colloidal system is subject is the dipole interaction. The dipole interaction is the classical one in the special case where all dipole
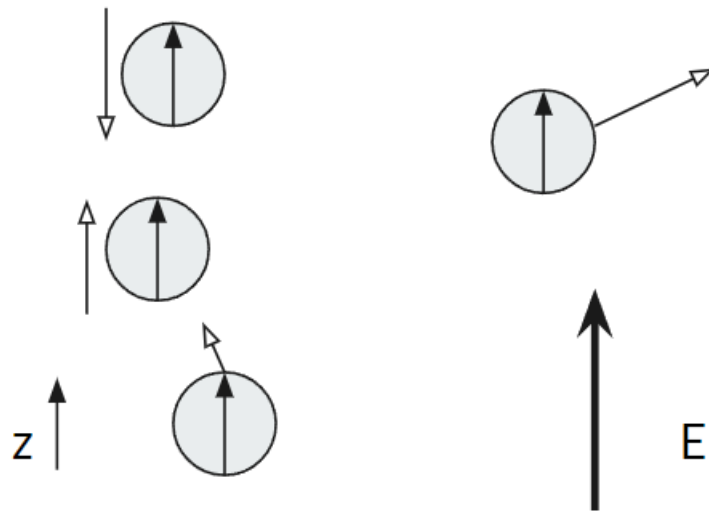
Figure 1.3: A depiction of the behaviour of colloids subject to the dipole interaction. Empty arrowheads represent directions of relative particle motion, and filled arrowheads represent direction of polarisation. Chains form along the z-axis, which attract at short distances and repel at large distances.

moment vectors are aligned with the electric field. This interaction arises when the system is subject to an external electric field, and the colloidal particles and solvent polarize. Owing to a mismatch in the dielectric constant between solvent and colloidal particles, the overall effect is equivalent to placing point dipoles at the centres of all the colloidal particles. The dipoles all point in the same direction, up along the now-ignorable electric field. The dipole-dipole interaction is depicted in Figure 1.3. In experiment, the induced dipole moment constantly changes direction from $+\hat{z}$ to $-\hat{z}$, due to the alternating current which produces the electric field, but the average magnitude of this moment remains constant. In simulation, both the direction and magnitude are kept constant, but the cell is simulated with periodic boundary conditions.

The dipole-dipole interaction can be written in terms of the interaction energy

between dipoles $\vec{p}_1$ at the origin and $\vec{p}_2$ at position $\vec{r}$, and the force on $\vec{p}_2$, as [6],

$$U_d(r) = \Lambda \left(\frac{\sigma}{r}\right)^3 [\vec{p}_1 \cdot \vec{p}_2 - 3 (\vec{p}_1 \cdot \hat{r}) (\vec{p}_2 \cdot \hat{r})]$$

$$\vec{F}_d(r) = \frac{3\Lambda\sigma^3}{r^4} \left[(\vec{p}_1 \cdot \hat{r}) \vec{p}_2 + (\vec{p}_2 \cdot \hat{r}) \vec{p}_1 + (\vec{p}_1 \cdot \vec{p}_2) \hat{r} - 5 (\vec{p}_1 \cdot \hat{r}) (\vec{p}_2 \cdot \hat{r}) \hat{r}\right] \tag{1.5}$$

In the simulated system, $\vec{p}_i = p\hat{z}$; all dipoles are aligned in order to simulate the uniform electric field. Λ is the strength of the dipolar interaction. Experimentally [3],

$$\Lambda p^2 = \frac{1}{16}\pi\epsilon_0\epsilon_s\sigma^3\beta^2 E_0^2 \tag{1.6}$$

where ϵ_0 is the permittivity of free space, ϵ_s is the permittivity of the solvent, ϵ_c is the permittivity of the colloid, and the dielectric mismatch β is given by [7]:

$$\beta = \frac{-1 + \epsilon_c/\epsilon_s}{2 + \epsilon_c/\epsilon_s} \tag{1.7}$$

Formally, the reduced interaction strengths $\tilde{\epsilon}/k_BT$ and $p^2\Lambda/k_BT$ are varied, where it is assumed that all particles have the same dipole moment, i.e., $|\vec{p}_i| = p$. In the simulation, k_BT is kept constant by a numerical thermostat to a value of unity, barring small equilibrium fluctuations in T. Results are reported in terms of dimensionless attractive well depth ϵ and dimensionless dipole moment $\mu = \sqrt{p^2\Lambda/k_BT}$, which govern the polymer concentration and electric field strength, respectively.

Chapter 2

Methods

2.1 Molecular Dynamics Simulation

The general algorithm for performing a molecular dynamics simulation is as follows [8]:

1. Initialise the particle positions and velocities and system parameters (e.g. dipole strength, well-depth). Positions are usually initialised on a regular array for simplicity, and velocities are generated randomly from a distribution, normalised according to the desired temperature or internal energy of the system.

2. At each timestep:

   (a) Determine the forces between particles.

   (b) Integrate Newton's equations using a numerical integrator, and update the particle positions and velocities according to the calculated force.

   (c) Accumulate thermodynamic averages of the system, such as the energy.

   (d) Increment the time variable.

3. Compute thermodynamic averages over all timesteps.

The simulation starts by initialising particle positions on a regular array, and randomly assigning velocities. The contrived array naturally leads to an unstable state, so the system must be brought to equilibrium by allowing the simulation to run for long simulation time, until potential energy stabilises, signalling the end of the transient phase of the simulation where forces and velocities are very large. The length of this process is variable, depending on system parameters. In general, systems with higher magnitude of ϵ and μ, which lead to increased potential energy, will have longer relaxation times. The molecular dynamics software LAMMPS (Large-scale Atomic/Molecular Massively Parallel Simulator), developed by the Sandia Corporation, was used for all simulations.[9]

To simulate the canonical ensemble, particle velocities must be modified in comparison to the purely Newtonian time evolution, in order to maintain the desired temperature. [8]. The Nosé-Hoover thermostat method was used within LAMMPS to maintain temperature. One must also be prudent about the choice of the time constant, which determines how quickly the algorithm acts to bring the system to the desired temperature. A fast-acting thermostat can result in unphysical transients of the system.

2.1.1 The Verlet Algorithm

The molecular dynamics solution of the many-body problem treats motion of particles governed by Newton's laws as ordinary differential equations:

$$\frac{dy}{dt} = v(t) \tag{2.1}$$

$$\frac{dv}{dt} = a(t) = F(t)/m \tag{2.2}$$

$$\tag{2.3}$$

where the force is derived as the negative gradient of some potential energy function.

To solve the differential equations, the theoretical many-dimensional integral turns into a discretised numerical integrator. Such discretised methods require careful analysis of how error propagates with each step. Fortunately, several algorithms have been developed and analysed for stability, such as the "velocity" variant of the Verlet algorithm [10]:

$$x_{n+1} = x_n + v_n \Delta t + \frac{1}{2} a_n (\Delta t)^2 \tag{2.4}$$

$$v_{n+1} = \frac{1}{2}(a_{n+1} + a_n)\Delta t \tag{2.5}$$

The Verlet algorithm has associated global error of order three for the position and order two for the velocity [10]. Absolute error minimisation in the trajectory is not the goal of molecular dynamics simulations, since in any case atomic trajectories are highly sensitive to perturbation, and the equilibrium properties sought from molecular dynamics methods are usually averaged over the ensemble and/or the time series, which obscures this sensitivity[11]. The time step Δt is ideally as large as possible while maintaining conservation of energy within a specified tolerance. Several typical
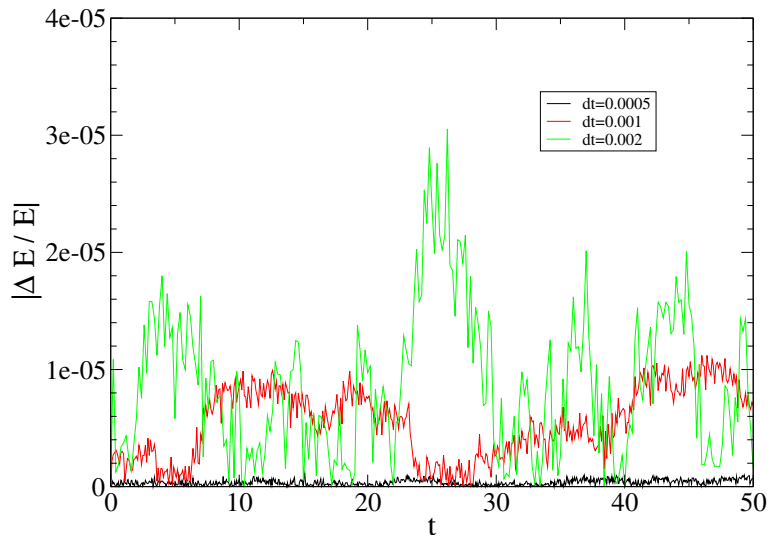
Figure 2.1: A graph of the relative change in energy from the initial energy of a system with parameters $\epsilon = 0$, $\mu = 0$, and $\phi = 0.1$, run in the microcanonical ensemble over time. The time step $dt = 0.0005$ gave the most uniform energy conservation of the time steps tested.

values for the molecular simulation timestep were tested for energy conservation in the microcanonical ensemble over an elapsed simulation time of $t = 50$, after the system had been brought to equilibrium in the canonical ensemble. The initial energy was subtracted from the energy at time t to get $\Delta E(t)$. The results are shown in Figure 2.1

For these simulations, according to these results, a timestep of $dt = 0.0005$ was used. This time step may seem conservative, however most initial configurations begin with very large transient forces, especially at high dipole moment and large well depth, so care was taken not to "lose atoms," by displacing them by more than the length of the simulation box in a short time interval, or incur large errors in the equilibration phase of these simulations, due to the large displacements resulting from these excessively large forces.

Additionally, to remove edge effects, a simulation box is defined with periodic
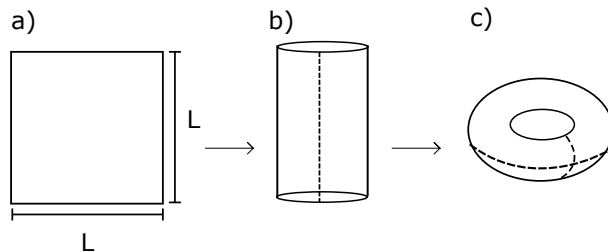
Figure 2.2: An illustration of periodic boundary conditions in a square simulation box of length L. In a), a particle moving towards the edge of the simulation box would collide with the wall and be sent back into the box elastically. In b), the particle would still collide with the wall at the top or bottom, but the left and right edges have been joined at the dashed line, so a particle approaching this line would continue along its current trajectory. In c), there are no longer any walls with which the particle may collide, so a single particle moving in this topology continues on its current trajectory forever.

boundary conditions. The box is replicated over many periodic images, so that a particle approaching the edge of the box is not reflected backward, but continues on its path at the opposite edge of the box. In two dimensions, for example, this is equivalent to taking a rectangular simulation box, and wrapping the left edge around to meet the right, and the top to meet the bottom, turning the square into the surface of a torus. This is depicted in Figure 2.2. Note that this example is simply a geometric homomorphism. Periodic boundary conditions preserve straight-line geodesics and zero curvature.

2.2 Ewald Treatment of the Dipole Interaction

For the long-range dipole interaction, the Ewald summation technique is employed. This method sidesteps the truncation associated with pairwise interaction over periodic boundaries by using periodic images of the system. That is, since the dipole interaction must necessarily act over a range much larger than the simulation box, the energy must depend on contributions from *all* replicated images. In the absence

of charge, the sum takes the form [11][12]:,

$$E(\vec{r}_1, ..., \vec{r}_N) = \frac{1}{2} \sum_{\vec{L}} \sum_i \sum_j (\vec{p}_i \cdot \nabla_i)(\vec{p}_j \cdot \nabla_i) \times \left(\frac{1}{|\vec{r}_i - \vec{r}_j + \vec{L}|} \right), \qquad (2.6)$$

where terms with $\vec{L} = 0$ and $i = j$ are omitted.

Of course, this sum can not be computed to the required degree of precision easily in real space. The Ewald method involves rewriting the above expression in terms of separate sums over real space and reciprocal space that involve functions that rapidly decay in their respective spaces. A more detailed description of the procedure and resulting expressions can be found in Refs. [11] and [12].

2.3   The Radial Distribution Function

The radial distribution function, termed the pair-distribution function in some texts, of a configuration of particles is defined as the probability of finding a particle at radial distance r from another particle, relative to an uniformly distributed, "random" system [13]. The two-dimensional case is depicted in Figure 2.3

To derive the radial distribution function, first consider a general n-particle distribution, beginning with the canonical distribution [14]:

$$f_0^{(n)}(\vec{r}^N, \vec{p}^N) = \frac{1}{h^{2N} N!} \frac{e^{-\beta H}}{Q_N} \qquad (2.7)$$

where H is the system Hamiltonian and Q_N is the canonical partition function:

$$Q_N = \frac{1}{h^{3N} N!} \iint e^{-\beta H} d\vec{r}^N d\vec{p}^N \qquad (2.8)$$
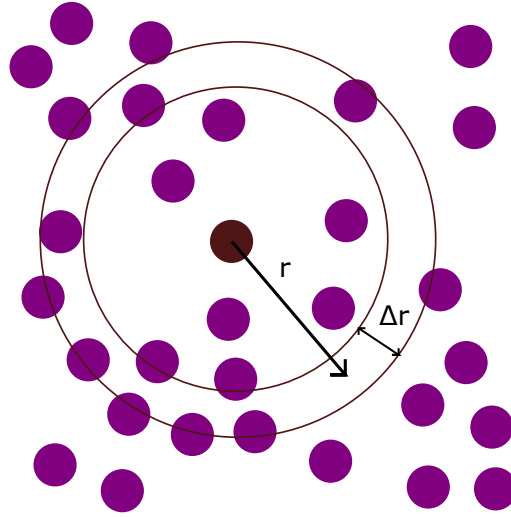
Figure 2.3: A depiction of how the radial distribution function is determined. Each particle, in turn, is considered to be the central particle (dark red). The number of particles (purple) in a thin neighbour shell Δr is calculated, and is assigned as the value of g for the radial distance r. Then, these r-values are averaged over the entire ensemble, and compared with an evenly distributed system.

$f_0^{(n)}$ can be written as the product of the *n-particle density* $\rho_N^{(n)}(\vec{r}^n)$, which is the probability of finding n particles of the system with coordinates in the volume element $d\vec{r}^n$, independent of the positions of the other particles and of all momenta:

$$\rho_N^{(n)}(\vec{r}^n) = \frac{N!}{(N-n)!}\frac{1}{Z_N}\int e^{-\beta V_N}d\vec{r}^{(N-n)} \tag{2.9}$$

and the product of n independent Maxwell distributions, independent of r:

$$f_M^{(n)}(\vec{p}^n) = \frac{1}{(2\pi m k_B T)^{3n/2}}\exp\left(-\beta\sum_{i=1}^{n}\frac{|\vec{p}_i|^2}{2m}\right) \tag{2.10}$$

The n-particle density is such that

$$\int \rho_N^{(n)}(\vec{r}^n)d\vec{r}^n = \frac{N!}{(N-n)!} \tag{2.11}$$

The n-particle distribution is defined in terms of these particle densities as:

$$g_N^{(n)}(\vec{r}^n) = \frac{\rho_N^{(n)}(\vec{r}_1, ..., \vec{r}_n)}{\prod_{i=1}^{n} \rho_N^{(1)}(\vec{r}_i)} \tag{2.12}$$

The *radial* distribution is the 2-particle distribution function, and depends only on the separation between particles. From the above,

$$g_N^{(2)}(\vec{r}_1, \vec{r}_2) = \frac{\rho_N^{(2)}(\vec{r}_1, \vec{r}_2)}{\rho_N^{(1)}(\vec{r}_1)\rho_N^{(1)}(\vec{r}_2)}, \tag{2.13}$$

and so the radial distribution may be written as an ensemble average over pairs of particles [15]:

$$g(r) = \rho^{-2} \left\langle \sum_i \sum_{j \neq i} \delta(\vec{r}_i)\delta(\vec{r}_j - \vec{r}) \right\rangle = \frac{V}{N^2} \left\langle \sum_i \sum_{j \neq i} \delta(\vec{r} - \vec{r}_{ij}) \right\rangle. \tag{2.14}$$

In the discretised treatment, in place of delta functions, a histogram is created for a series of spherical or circular shells of width Δr, and all particles within the shell $r \in [R, R + \Delta r]$ are counted for a shell of radius $R + \frac{1}{2}\Delta r$.

The radial distribution function serves as a quantitative measure of the order of a system. For instance, a sharp peak in $g(r)$ indicates increased local order, as it means less variance in the distance from a central particle and its neighbours within some specified neighbour shell. One can compare the 2D and 3D formulations of the radial distribution function to surmise whether such an increase in order is replicated in a particular direction. In this case, the goal is to assess whether changes in peak heights are replicated in the z-direction - that of the electric field. In order to construct a 2D radial distribution function from a 3D configuration, one considers the x and y coordinates of all particles within a slab of thickness σ in the z-direction.
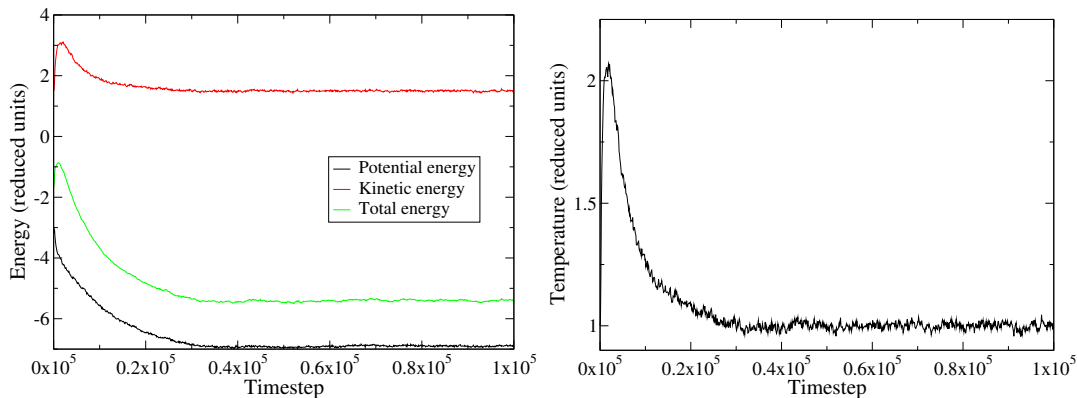
Figure 2.4: Time series showing how the kinetic, potential, and total energies (left), and the temperature (right) evolve with time when run in the canonical ensemble, with $\epsilon = 1$ and $\mu = 2$. There is a transient spike in energy at the beginning of the time series, but all curves flatten out after some time. The temperature also has some transient behaviour, as well as some fluctuations about its baseline, but once equilibrated, maintains stable temperature of about 1 in reduced units.

2.4 Computation

The LAMMPS molecular dynamics software was used to generate all trajectory and thermodynamic data for these simulations. Each system was initialised on a cubic lattice, with velocities randomly generated according to a Gaussian distribution.

To gather data, the system was run in the canonical ensemble, and configurations of particles were output every 50 time steps. The systems were brought to equilibrium over 50 000 time steps, then data was produced over another 50 000 steps. Reported quantities were the per-particle kinetic, potential, and total energies, and the pressure and temperature. All quantities were reported in reduced units as described above. An example of such time series of potential, kinetic, and total energies is shown in Figure 2.4.

For use with LAMMPS, the colloid potential is provided in tables of sampled triplets of radial position, potential, and force, since the colloid potential is not a standard potential provided by LAMMPS. Tables were generated for various well

depths ϵ, to mimic increased effective attraction with increased polymer concentration in experiment. The table was interpolated with cubic splines. Well depths ranged from 0 to 3.5, in increments of 0.25, and a resolution of 0.001 was used. In the special case of zero polymer, the potential was cut and shifted to zero at the minimum. This was done to maintain hard-sphere repulsion.

The (dimensionless) dipole moment μ was varied from 0 to 2.0, in increments of 0.25. Two packing fractions were tested: $\phi = 0.1$ and $\phi = 0.2$. In the experimental analog, $\phi = 0.1$ was the packing fraction reported. However, the effective charge on the colloidal spheres causes the effective packing fraction to be larger, so a system with $\phi = 0.2$ was simulated as well, to bracket this parameter.

Chapter 3

Results

3.1   Phase Diagrams

Figure 3.1 shows the rudimentary behaviour of a colloidal system at equilibrium with increasing dipole moment in three dimensions, for a system with $\phi = 0.1$ and $\epsilon = 1$[1]. The system is fluid-like at low dipole moment, while at higher dipole moment, it is clustered, with some isolated chains throughout, and at very high dipole moment (much higher than used in Semwal[3], without accounting for charge and inter-polymer potential effects), one sees very tightly packed crystallites with most of the chains seen at lower dipole moment aggregated into larger crystallites

A 2D configuration snapshot was taken from each state point trajectory at equilibrium. These were produced by taking the x and y coordinates of all particles within a slab of thickness σ, and collapsing the z-coordinates into a single plane. The point of view of these snapshots is looking down the z-axis. This was done for packing

---

[1]These figures, and all other 3D particle configurations in this paper were generated with Visual Molecular Dynamics. VMD is developed with NIH support by the Theoretical and Computational Biophysics group at the Beckman Institute, University of Illinois at Urbana-Champaign.
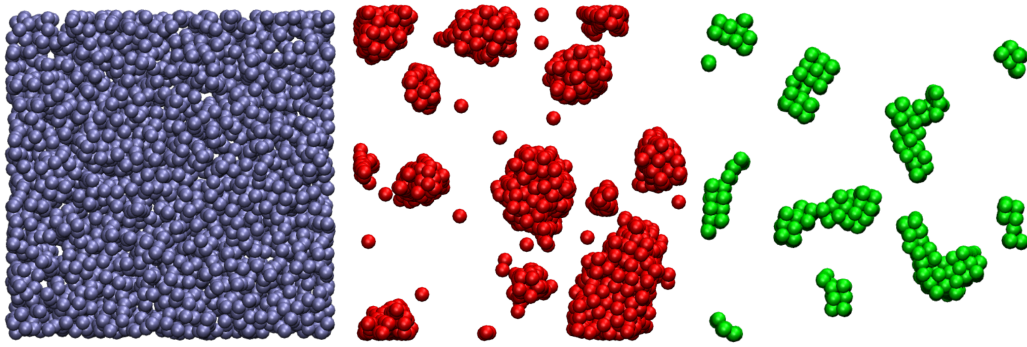
Figure 3.1: Equilibrium configurations of a colloidal systems with $\phi = 0.1$, $\epsilon = 1$ fixed, and, from left to right, $\mu = 1, 2, 5$

fractions $\phi = 0.1$ and $\phi = 0.2$ to generate Figures 3.2 and 3.3 respectively. These are two-dimensional graphs with increasing ϵ from top to bottom and increasing μ from left to right. ϵ varies from 0 to 3.25 in steps of 0.25, and μ increases from 0 to 2 in steps of 0.25.

Assessing Figure 3.2 qualitatively, one sees a transition from fluid-like behaviour at the top left, to discrete crystallites or clusters at the bottom right, with a distinct phase boundary near the diagonal. Near the phase boundary, one notes more single-particle chains surrounding the crystallites. As seen in experiment, when the dipole moment is high, the system need not have a strong depletion interaction, i.e. a high value of ϵ, in order to form crystals. That is to say, the threshold of ϵ at which the system crystallises tends to decrease with increasing μ. Similarly, one sees a greater propensity to form clusters at high values of ϵ, and so it takes a much weaker dipole moment to cause the system to crystallise, as the colloids are already quite tightly packed together. Unlike the experiment, one does not see a transition to the highly disordered gel phase at high values of ϵ. There were also no large, percolating clusters observed. Semwal uses a packing fraction of $\phi = 0.1$[3], however the phase diagram produced by using this value in simulation showed clusters much too small to be comparable. The effective charge in the experiment could have led to an effectively

larger packing fraction, so the simulations were also run for $\phi = 0.2$. Comparing the morphology produced by this higher packing fraction, one sees better agreement.

Likewise, there appears to be a transition from fluid to highly ordered crystal in Figure 3.3. However, by surveying the rightmost column, corresponding to $\mu = 2$, one clearly sees yet another transition to a less ordered crystal structure, which is not so clear in the $\phi = 0.1$ case. This observation is corroborated in the 3D slices of the $\phi = 0.2$ system. In Figure 3.6, one sees this clearly as μ increases left to right. Particularly in the top row, one sees the chains ordering, then disordering again.

In Figure 3.3, for $\phi = 0.2$ there is also a clear phase boundary between fluid and crystal structure. However, the crystals are remarkably larger and more contiguous. This is certainly due to the increased packing fraction, which is a closer match to the experimental packing fraction in Semwal[3].

The effects of increasing dipole moment, at $\epsilon = 0$, and increasing well depth, at $\mu = 0$, become even more concrete in assessing Figures 3.4 and 3.5 respectively. These show the behaviour at equilibrium of a system at packing fraction $\phi = 0.1$. In Figure 3.4, looking down the x-axis, one sees the formation of chains along the direction of polarisation as the dipole moment increases, leading to large voids in the system looking down the z-axis. Correspondingly, one sees a reduction in the peak height of the 2D radial distribution function, as order increases along the z-axis, which effectively reduces the area packing fraction in the x-y plane. Additionally, the chains repel in the x-y plane, also reducing the effective packing fraction. There is also a dramatic increase in the peak height of the 3D radial distribution function, which corresponds to the increased order in z. In Figure 3.5, one sees the isotropic formation of clusters as the well-depth is increased without the interference of the dipole moment. As expected, one notes an increase in peak height of *both* 2D and

3D $g(r)$, as the colloids succumb to the depletion interaction and stick together, such that particles tend to have more neighbours in all directions.

The most remarkable result is seen in Figure 3.6. This figure shows systems with packing fraction $\phi = 0.2$ and $\mu = 2$, at values of $\epsilon = 0.25$, 0.5, 1.5, and 3, increasing from left to right. The first row shows the point of view from the x-axis, perpendicular to the direction of polarisation. At each state point, chains have formed along the z-axis as expected, and from $\epsilon = 0.25$ to $\epsilon = 0.5$, one sees tighter clustering of these chains. Then, the chains attain a high degree of order at $\epsilon = 1.5$. This progression is confirmed by studying the peaks in the 3D radial distribution function beyond the first; these secondary peaks are especially pronounced for $\epsilon = 1.5$, meaning decreased variation in distance to particles within more distant neighbour shells. Then, these secondary peaks become much less pronounced as ϵ increases to 3, confirming what one could infer by visual inspection of the corresponding x-axis view of the system: the system has become more disordered. One sees a similar trend upon the study of the second row of this figure, the view parallel to the z-axis, and the 2D radial distribution function. This time, the increase, then decrease is seen in the first peak as well as subsequent peaks.

A more quantitative analysis is performed by inspecting the trend of the first 2D radial distribution function peak height with variate ϵ and μ, as is done in Figures 3.7 and 3.8 respectively. In Figure 3.7, at weak dipole moment, one notes monotonic increase in the peak height with ϵ at each value of μ, with a sharper increase occurring around $\epsilon = 2$, consistent with the observation of clusters forming near this value of ϵ even at low dipole moment in the phase diagram Figure 3.3. At high dipole moment, in particular at $\mu = 2$ in the graph, one notes a characteristic increase to a maximum peak height at around $\epsilon = 1.5$. This is the state point with the highly ordered crystal
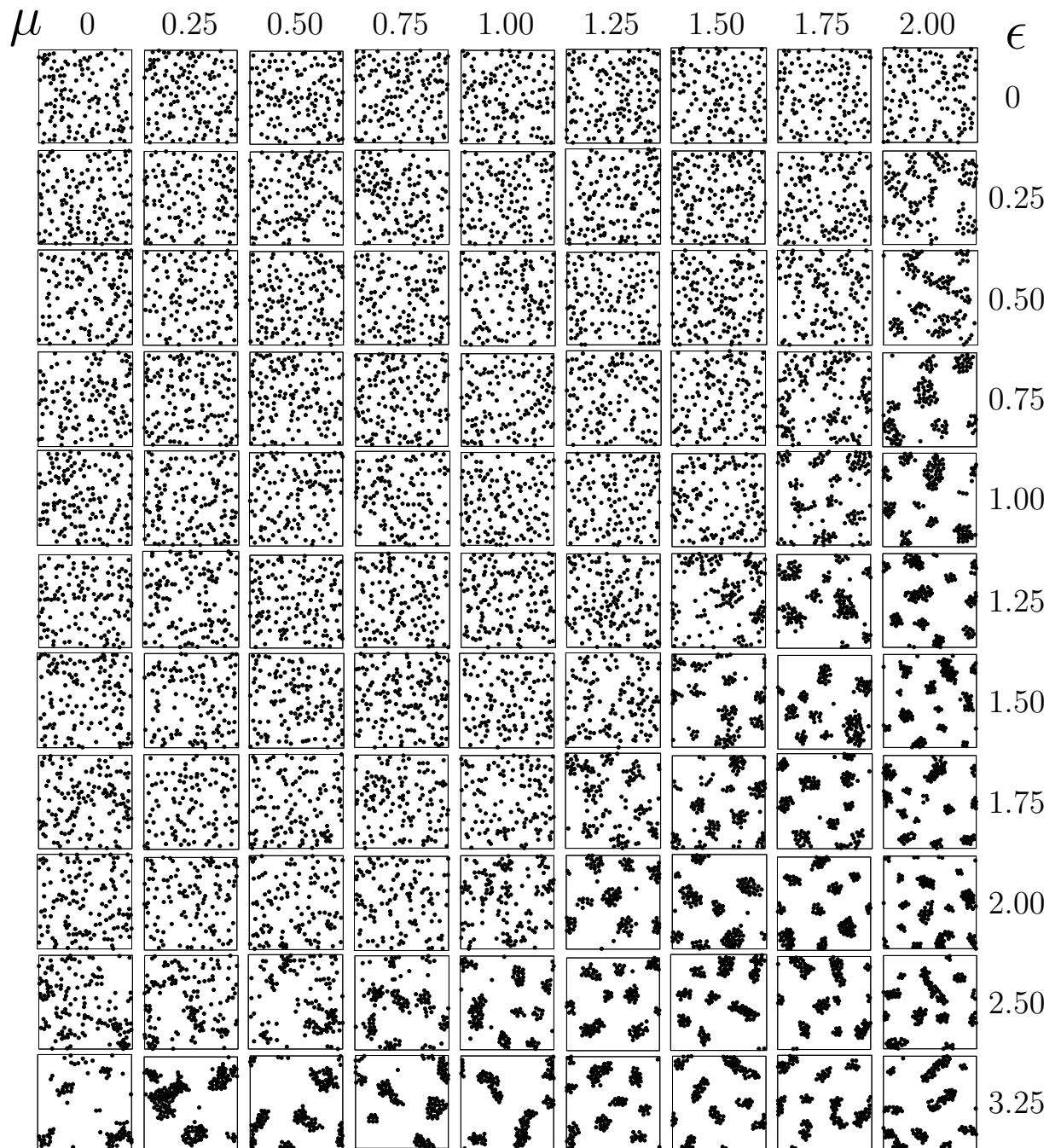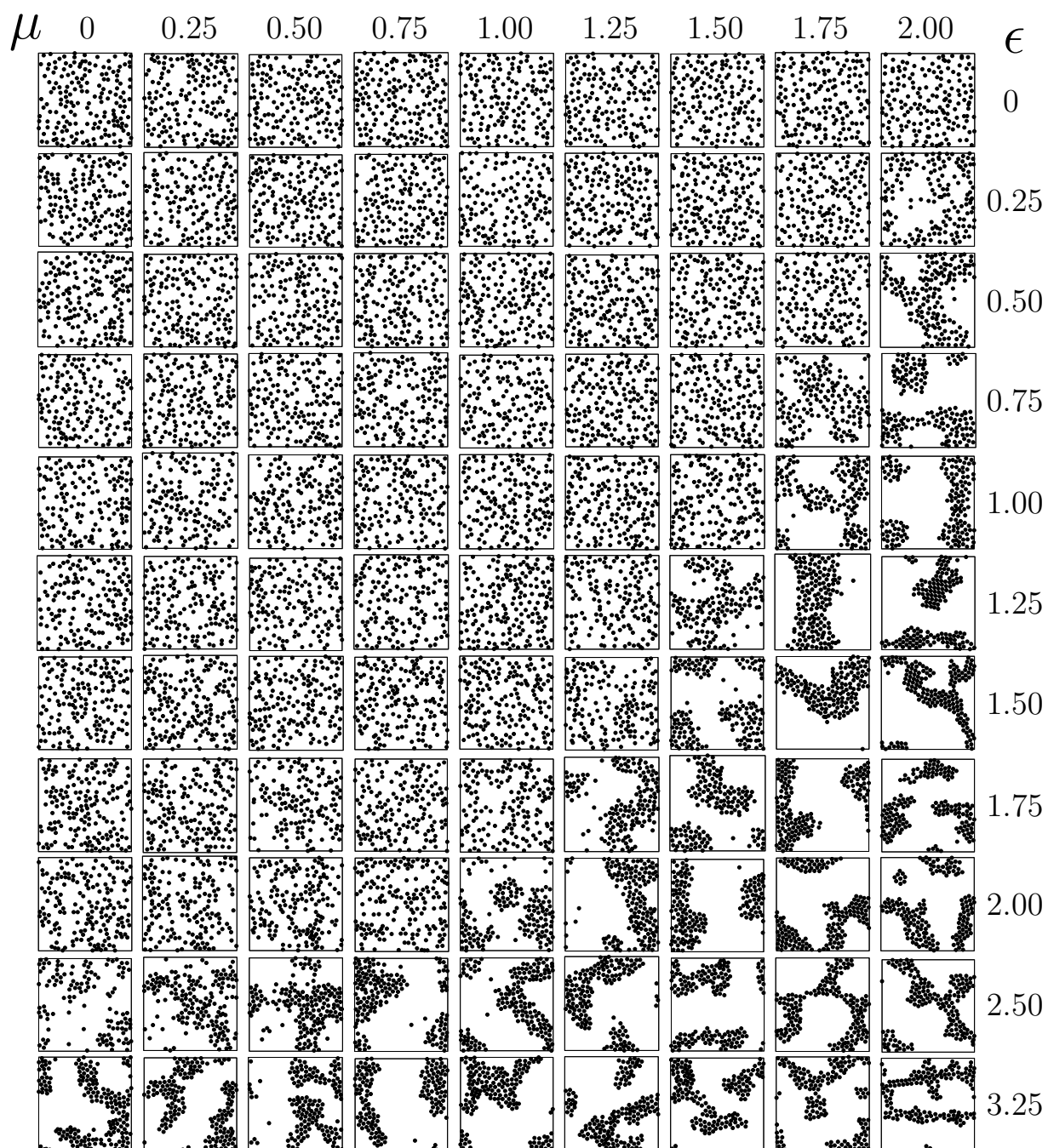
Figure 3.2: 2D configurations looking down the z-axis, for $\phi = 0.1$. From top to bottom, ϵ increases from 0 to 3.25, as labelled on the right, and μ increases from left to right, from 0 to 2, in increments of 0.25.

Figure 3.3: 2D configurations looking down the z-axis, for $\phi = 0.2$. From top to bottom, ϵ increases from 0 to 3.25, as labelled on the right, and μ increases from left to right, from 0 to 2, in increments of 0.25.
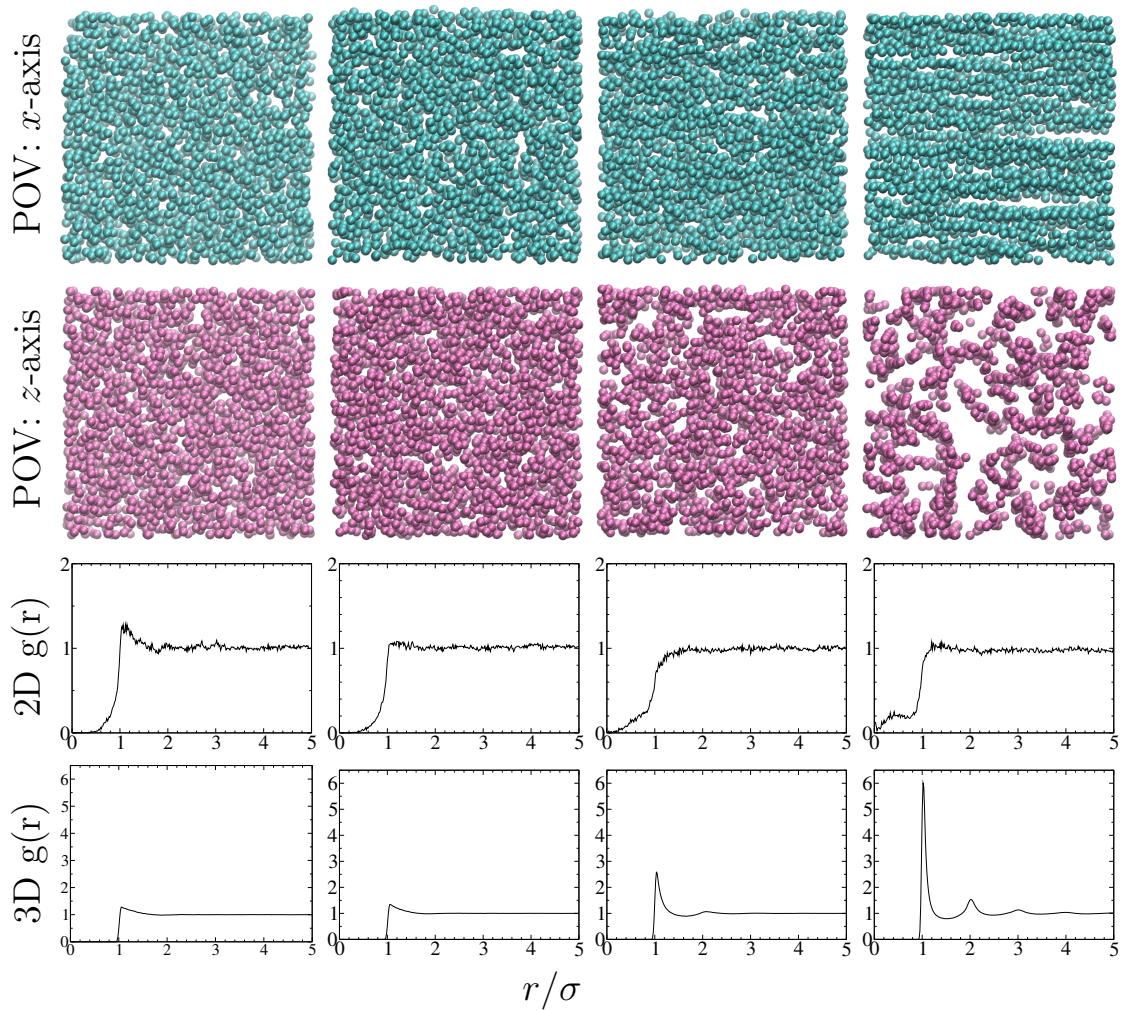
Figure 3.4: Effect of increasing μ on the system with $\epsilon = 0$, $\phi = 0.1$. The top row shows the point of view (POV) looking down the x-axis, the second row shows the point of view looking down the z-axis, the third shows the 2D radial distribution function, and the fourth the 3D radial distribution function. From left to right, these are the state points with $\mu = 0$, 0.75, 1.5, and 2.
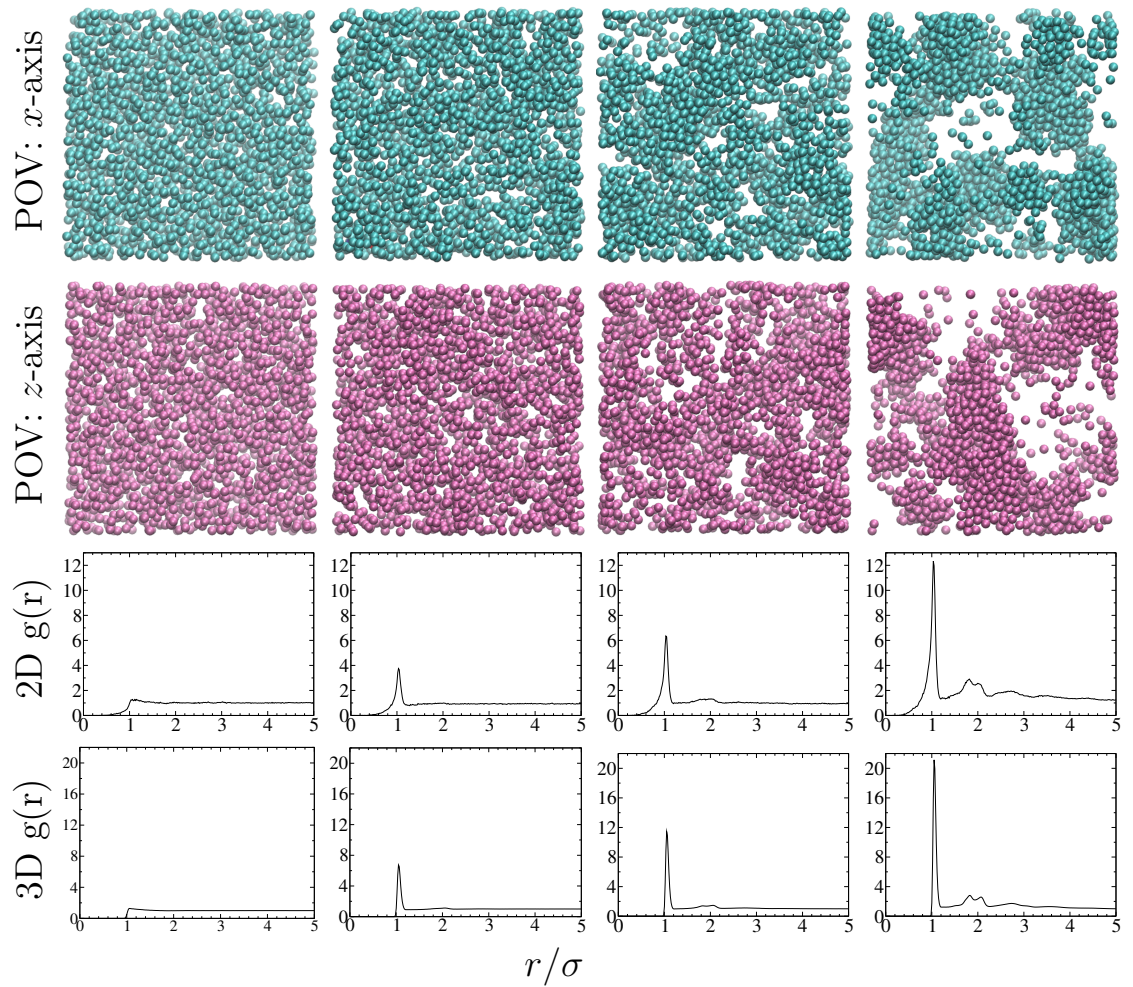
Figure 3.5: Effect of increasing ϵ on the system with $\mu = 0$, $\phi = 0.1$. From left to right, these are the state points with $\epsilon = 0$, 2, 2.5, and 3
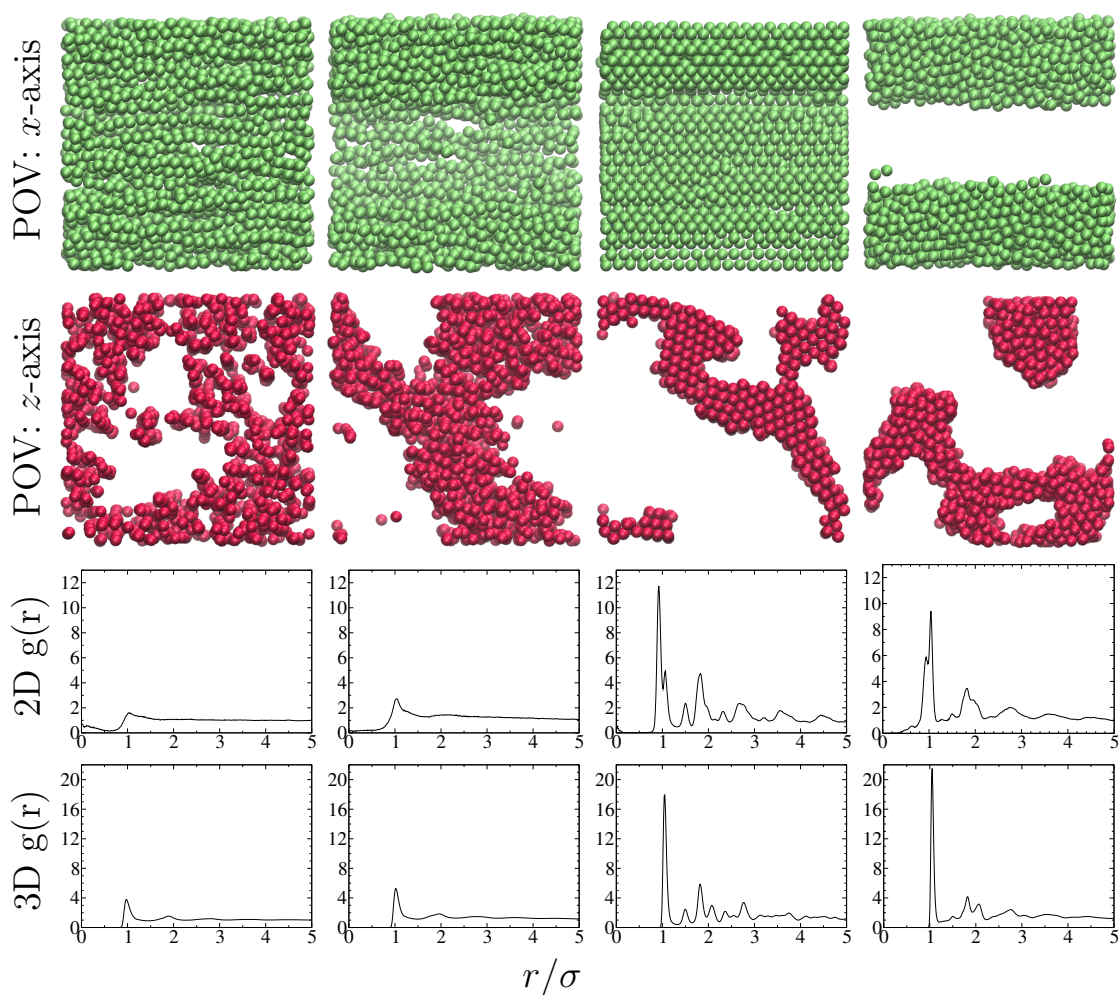
Figure 3.6: Equilibrium configurations of the colloidal system with $\mu = 2$, $\phi = 0.2$, and their associated 2D and 3D radial distribution functions. From left to right, these are the state points with $\epsilon = 0.25$, 0.5, 1.5, and 3.
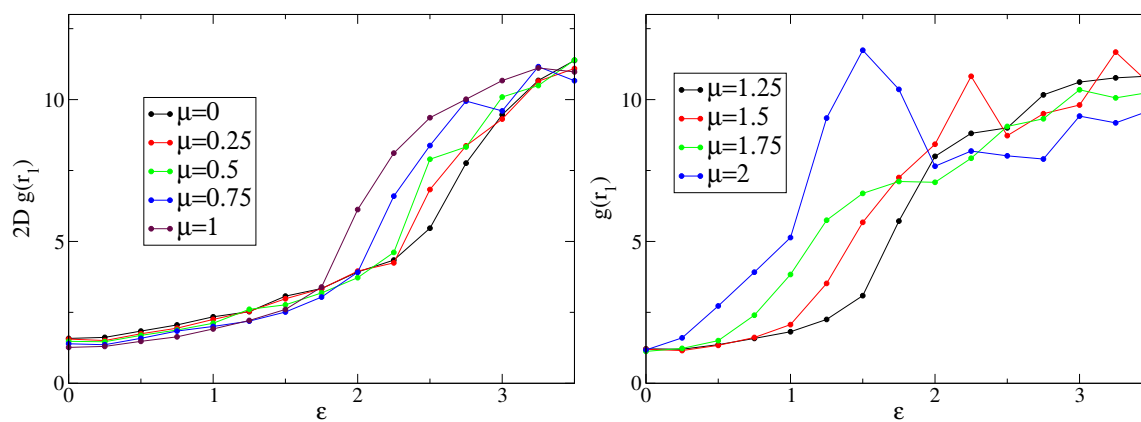

Figure 3.7: Peak heights near $r = 1$ for constant μ and varying ϵ, in 2D.

phase, as noted in the discussion of Figure 3.6. Then, the peak height decreases again as ϵ is increased further, to a trend with a much flatter slope. This mirrors the observation of decrease in crystal order beyond the highly ordered crystal at $\epsilon = 1.5$ and $\mu = 2$, noted qualitatively above. This behaviour of the 2D radial distribution function is also remarked in Semwal[3]. This appears to confirm the efficacy of the simulation in replicating the reintroduced disorder, as well as demonstrate that the competition between the isotropic and anisotropic interactions appears to be a primary influence in this disordering.

Furthermore, inspection of Figure 3.8 reveals an initial decrease in the 2D peak height with μ at low values of ϵ, followed by a sharp increase, also as observed in Semwal[3]. The middle plot once again corroborates the trend of increasing, then decreasing order, as the curves $\epsilon = 1.25, 1.5, 1.75$ appear concave up, as seen in the left figure, but the curves $\epsilon = 2, 2.25$ appear concave down, showing that beyond some critical value of ϵ, the 2D peak height achieves a maximum in μ before decreasing. The rightmost plot shows that, farther from this phase boundary, one sees a monotonic decrease in the 2D peak, and therefore the order. This plot also exhibits a divergence from experiment, as in experiment one would expect a much more dramatic decrease in this peak height, as the system enters a gel state. In simulation, the system exhibited disordering, but remained in either a crystal or cluster phase for those state points beyond the phase boundary at comparable values to those in Semwal[3].
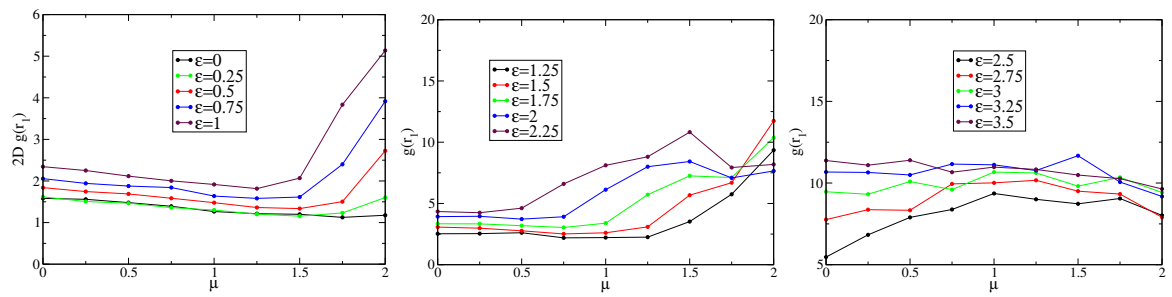
Figure 3.8: Peak heights near $r = 1$ for constant ϵ and varying μ, in 2D.

Chapter 4

Conclusions

The results obtained via simulation appear to replicate key aspects of the experimental system, but diverge from observed experimental behaviour at high values of the well depth. Phase transitions from fluid, to fluid-like clusters, to crystalline clusters, to partially ordered clusters were observed as in experiment. However transition back to a highly disordered state was not observed as in experiment at similar state points. Correspondingly, the trend of increase, then decrease in the local order of the system was observed and quantified by the radial distribution function. Most notably, the reintroduction of disorder as seen in experiment was replicated by modelling only the depletion and dipole-dipole interactions, which suggests that the competition between the isotropic and anisotropic potentials plays a primary role in the reintroduction of disorder.

However, as the system does not return to the highly disordered state at high state points, it is apparent that there are other factors than the potentials modelled which affect the degree to which the system becomes disordered beyond a certain value of ϵ. Semwal notes a critical polymer concentration c^* beyond which order does not tend

to increase with concentration[3], so it is possible that the simulated model is not sufficient for replicating more than superficial reduction in order beyond this critical value. Further simulations could be conducted in which effective charge is accounted for, which can be done directly by specifying effective charge in LAMMPS. This would add yet another isotropic interaction which could serve to disrupt crystalline structures and replicate the return to fluid or gel state as seen in experiment. For further increased fidelity, it may be necessary to develop a correction to the colloid potential used herein to account for the interaction between polymers at high field and high concentration. Similarly, since the morphology was seen to be vastly different with the two packing fractions tested, yet neither completely accurately replicated the experimental system, future work could involve running similar simulations at a range of packing fractions between $\phi = 0.1$ and 0.2. It may not be necessary to model charge directly if the effective charge is sufficiently accounted for by an appropriate packing fraction. One seeks interstitial behaviour between the small clusters observed at high dipole moment and large well depth at $\phi = 0.1$ and the large, percolating clusters seen at those state points with $\phi = 0.2$.

Further assessments of the order could be made by way of an order parameter, as in Semwal[3], to more precisely determine how well simulated results replicate experimental results at various state points, and determine at precisely which well depth the simulated system diverges from experiment. Likewise, one could examine the behaviour of secondary peaks in 3D g(r) to bolster the observation of decreased order in the z-direction at high dipole moment and large well depth.

Bibliography

[1] Mary Ann Mansigh Karlsen. *World Scientific Symposium in Honor of Dr Berni Alder's 90th Birthday*, chapter The Early Years of Molecular Dynamics and Computers at UCRL, LRL, LLL, and LLNL. World Scientific, 2015.

[2] Giovanni Battimelli and Giovanni Ciccotti. Berni alder and the pioneering times of molecular simulation. *The European Physical Journal H*, 43, 2018.

[3] Shivani Semwal, Ivan Saika-Voivod, and Anand Yethiraj. Dipolar depletion: the study of a field tunable colloid-polymer system. PhD Thesis, Memorial University (unpublished), 2021-2022.

[4] Sho Asakura and Fumio Oosawa. On interaction between two bodies immersed in a solution of macromolecules. *The Journal of Chemical Physics*, pages 1255–1256, 2 1954.

[5] Xipeng Wang, Simòn Ramìrez-Hinestrosa, Jure Dobnikar, and Daan Frenkel. The Lennard-Jones potential: when (not) to use it. *Physical Chemistry Chemical Physics*, 22:10624–10633, 2020.

[6] Pair_style LJ/long/dipole/long command. `https://docs.lammps.org/pair_dipole.html#pair-style-lj-long-dipole-long-command`. Accessed: 2021-11-30.

[7] Anand Yethiraj. Tunable colloids: control of colloidal phase transitions with tunable interactions. *Soft Matter*, pages 1099–1115, 7 2007.

[8] Daan Frenkel and Berend Smit. *Understanding Molecular Simulation*. Academic Press, 2 edition, 2002.

[9] A. P. Thompson, H. M. Aktulga, R. Berger, D. S. Bolintineanu, W. M. Brown, P. S. Crozier, P. J. in 't Veld, A. Kohlmeyer, S. G. Moore, T. D. Nguyen, R. Shan, M. J. Stevens, J. Tranchida, C. Trott, and S. J. Plimpton. LAMMPS - a flexible simulation tool for particle-based materials modeling at the atomic, meso, and continuum scales. *Comp. Phys. Comm.*, 271:108171, 2022.

[10] Harvey Gould, Jan Tobochnik, and Wolfgang Christian. *An Introduction to Computer Simulation Methods: Applications to Physical Systems.* Pearson, 3 edition, 2016.

[11] D.C. Rapaport. *The Art of Molecular Dynamics Simulation.* Cambridge University Press, 2 edition, 2004.

[12] Abdulnour Toukmaji, Celeste Sagui, John Board, and Tom Darden. Efficient particle-mesh ewald based approach to fixed and induced dipolar interactions. *Journal of Chemical Physics*, 113:10913–10927, 12 2000.

[13] Michael Plischke and Birger Bergersen. *Equilibrium Statistical Physics.* World Scientific, 3 edition, 2007.

[14] J.-P. Hansen and I.R. McDonald. *Theory of Simple Liquids.* Academic Press, 3 edition, 2006.

[15] M.P. Allen and D.J. Tildesley. *Computer Simulation of Liquids.* Clarendon Press, 1991.